Microwave Fluorescence Detection of Spin Echoes

E. Billaud,[1] L. Balembois,[1] M. Le Dantec,[1] M. Rančić,[1] E. Albertinale,[1] S. Bertaina,[2] T. Chanelière,[3] P. Goldner,[4] D. Estève,[1] D. Vion,[1] P. Bertet,[1,*] and E. Flurin[1,†]

[1]*Université Paris-Saclay, CEA, CNRS, SPEC, 91191 Gif-sur-Yvette Cedex, France*

[2]*CNRS, Aix-Marseille Université, IM2NP (UMR 7334), Institut Matériaux Microélectronique et Nanosciences de Provence, 13397 Marseille, France*

[3]*Université Grenoble Alpes, CNRS, Grenoble INP, Institut Néel, 38000 Grenoble, France*

[4]*Chimie ParisTech, PSL University, CNRS, Institut de Recherche de Chimie Paris, 75005 Paris, France*

(Received 30 August 2022; accepted 19 July 2023; published 8 September 2023)

Counting the microwave photons emitted by an ensemble of electron spins when they relax radiatively has recently been proposed as a sensitive method for electron paramagnetic resonance spectroscopy, enabled by the development of operational single microwave photon detectors at millikelvin temperature. Here, we report the detection of spin echoes in the spin fluorescence signal. The echo manifests itself as a coherent modulation of the number of photons spontaneously emitted after a $\pi/2_X - \tau - \pi_Y - \tau - \pi/2_\Phi$ sequence, dependent on the relative phase Φ. We demonstrate experimentally this detection method using an ensemble of Er^{3+} ion spins in a scheelite crystal of $CaWO_4$. We use fluorescence-detected echoes to measure the erbium spin coherence time, as well as the echo envelope modulation due to the coupling to the ^{183}W nuclear spins surrounding each ion. We finally compare the signal-to-noise ratio of inductively detected and fluorescence-detected echoes, and show that it is larger with the fluorescence method.

DOI: 10.1103/PhysRevLett.131.100804

Electron paramagnetic resonance (EPR) spectroscopy is the method of choice to characterize the concentration and properties of paramagnetic impurities in a sample [1]. EPR relies on the application of microwave pulse sequences to the spins, the most widely used being the Hahn echo $\pi/2_X - \tau - \pi_Y - \tau -$ echo [2]. Applied to an ensemble of N electron spins $S = 1/2$ with an inhomogeneously broadened Larmor frequency distribution, the Hahn echo sequence generates a transient buildup of macroscopic transverse magnetization S_Y, due to the rephasing of the spin dipoles at a time τ after the second pulse. Because the echo amplitude depends on multiple factors such as spin density, coherence time, and nuclear spin environment, spin-echo measurements are a cornerstone of EPR spectroscopy.

Spin echoes are usually detected by coupling the spins to a microwave resonator at frequency ω_0. The Larmor precession of the transverse magnetization S_Y induces the emission into an output waveguide of a phase-coherent microwave pulse of amplitude X_e and duration T_e, which is then amplified and detected [see Fig. 1(a)]. For samples with a low paramagnetic concentration such that $pN\Gamma_R T_e \ll 1$, the average energy emitted in this echo, $\langle X_e\rangle^2 \hbar\omega_0 \sim (pN)^2 \Gamma_R T_e \hbar\omega_0$, is a small fraction of the total energy stored in the spin ensemble $pN\hbar\omega_0/2$, Γ_R being the spontaneous emission rate of one spin into the waveguide and p the average spin polarization [3,4]. As a result, echoes are hard to detect with small-volume or low-concentrated samples, preventing pulsed EPR spectroscopy studies of microcrystals or individual cells for instance. This motivated intense research efforts for alternative detection schemes with enhanced signal-to-noise ratio (SNR), such as optical [5], electrical [6], or scanning-probe [7,8] detection of magnetic resonance. These methods are either system specific or have a low detection volume, which makes them less versatile than resonator-based detection. In parallel, it was recognized that superconducting quantum technology can be useful to increase the sensitivity of resonator-based inductive detection, by using small-mode-volume and high-quality-factor resonators to increase Γ_R through the Purcell effect [9–14], by cooling the sample at temperatures well below $\hbar\omega_0/k_B$ to polarize the spins ($p = 1$) and suppress thermal noise, and by using superconducting quantum-limited amplifiers [3,15–17]. Nevertheless, vacuum fluctuations in the echo detection mode, with standard deviation $\delta X_e = 1/2$, ultimately impose an upper limit $\langle X_e\rangle/\delta X_e \sim 2N\sqrt{\Gamma_R T_e}$ to the SNR reachable in inductively detected (ID) ESR.

In this Letter, we demonstrate a novel resonator-based echo detection method which can reach a higher SNR. We convert the transverse magnetization into a longitudinal one by adding a $\pi/2_\Phi$ pulse applied at the echo time, called the restoring pulse in the following, analogous to the optical detection of spin echoes [18,19]. The resulting phase-coherent modulation of the longitudinal magnetization $\langle S_Z\rangle = N/2\cos\Phi$ is detected by the incoherent microwave radiation—called the fluorescence signal—that the spins subsequently emit when they relax radiatively, at the rate

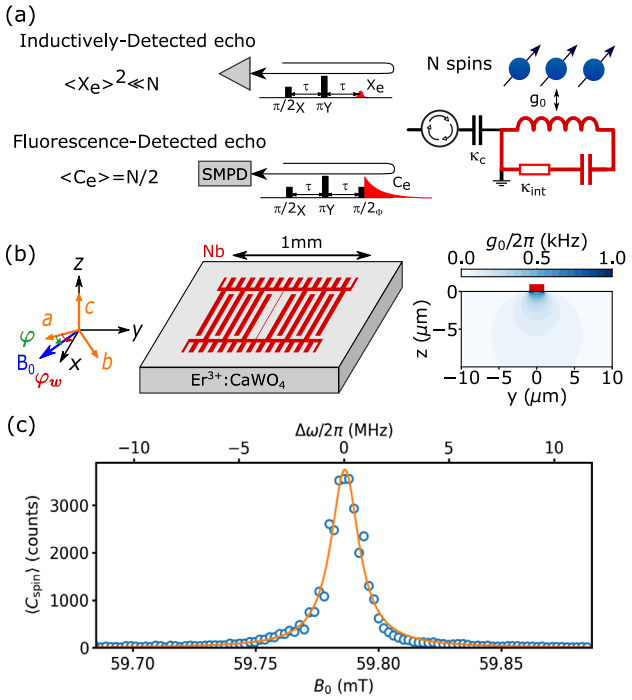

FIG. 1. Experiment principle and spectroscopy. (a) Schematic of the experiment. N spins are coupled (with strength g_0) to a resonator of frequency $\omega_0/2\pi = 6.999$ GHz damped by internal losses at a rate $\kappa_{\text{int}} = 3.6 \times 10^5$ s^{-1}, coupled to a transmission line at a rate $\kappa_c = 2 \times 10^6$ s^{-1}. In the ID echo detection scheme, a Hahn echo pulse sequence $\pi/2_X - \tau - \pi_Y$ is applied to the spins, inducing the emission of a coherent echo of amplitude $\langle X_e \rangle$ at time 2τ which is then amplified. In the FD echo detection scheme, a three-pulse sequence $\pi/2_X - \tau - \pi_Y - \tau - \pi/2_\Phi$ is used. The echo is detected by counting the incoherent photons emitted subsequently with a SMPD. The number of photons in the FD scheme $\langle C_e \rangle = N/2$ is much larger than in the coherent echo $\langle X_e \rangle^2$, explaining why a larger SNR can be reached with a low-noise SMPD. (b) Sketch of the niobium planar resonator fabricated on top of the $CaWO_4$ sample in the ab plane. The 630 μm-long wire is along the x axis ($\varphi_w = 51°$), and B_0 is in the ab plane ($\varphi = 30°$). The cross section of the sample below the 2 μm-wide wire (shown as a red rectangle) displays the spatial distribution of the coupling g_0, which we assume to be constant across the wire length. (c) Fluorescence-detected EPR spectrum of Er^{3+}: $CaWO_4$. The number of counts with background subtracted $\langle C_{\text{spin}} \rangle$ (open blue circles) is shown as a function of B_0 (bottom axis), also converted into frequency detuning from the center of the line (top axis). The solid line is a fit to a Lorentzian with FWHM 1.6 MHz. Data were obtained with SMPD1.

Γ_R, to their ground state equilibrium [see Fig. 1(a)]. Our new fluorescence-detected (FD) echo scheme can reach a higher SNR than ID for two reasons. First, in the regime where the dominant spin relaxation channel is radiative (the so-called Purcell regime [14]), the number of photons in the FD echo $\langle C_e \rangle = N/2$ is much larger than in the coherent echo $\langle X_e \rangle^2$. Second, these fluorescence photons can be detected noiselessly by using an ideal single microwave photon detector (SMPD) [4,20]. As a result, the SNR of a FD echo can in principle reach arbitrarily high values, and certainly much larger than for an ID echo. In this Letter, we measure a fluorescence-detected spin-echo signal from an ensemble of Er^{3+} ions in a scheelite crystal of $CaWO_4$ (a model system for EPR spectroscopy [21–25]) using a recently developed SMPD based on a transmon qubit [4,20], and we demonstrate a larger SNR than with inductive detection despite the nonidealities of our experiment.

The ground state of Er^{3+}: $CaWO_4$ is a degenerate doublet, and behaves as an effective electron spin $S = 1/2$ in the presence of a magnetic field B_0. The main components of its anisotropic gyromagnetic tensor $\gamma_\parallel/2\pi = 17.45$ GHz/T and $\gamma_\perp/2\pi = 117.3$ GHz/T depend on whether B_0 is applied parallel or perpendicular to the crystal c axis. Here we consider only the $I = 0$ erbium isotopes. $CaWO_4$ has a low nuclear-magnetic-moment density, since only the tungsten atoms have a stable spin-1/2 isotope (^{183}W, present at 14% natural abundance), with a low gyromagnetic ratio $\gamma_n/2\pi = 1.8$ MHz/T. The spin properties of paramagnetic rare-earth-ion-doped crystals were recently studied in the millikelvin regime, and shown to reach coherence times well above the millisecond [25–28]. In this Letter we use the same sample as in Ref. [25], a pure scheelite crystal with residual Er^{3+} concentration 7 μm^{-3} [29], enabling a quantitative comparison between results obtained by FD and by ID.

As shown in Fig. 1(a), the Er^{3+} ions are coupled to a planar superconducting microwave LC resonator deposited on top of the ab oriented crystal surface through the dipolar magnetic interaction with the magnetic component of the resonator field. The resonator geometry schematically depicted in Fig. 1(b) consists of a 2 μm-wide wire that acts as an inductance, in parallel with an interdigitated capacitor, leading to a frequency of $\omega_0/2\pi = 6.999$ GHz (resonator 1 in [25]). Because the magnetic field vacuum fluctuations $\delta\mathbf{B_1}(\mathbf{r})$ depend on the position $\mathbf{r} = (y, z)$ with respect to the inductance, the spin-photon coupling constant $g_0(\mathbf{r}) = \delta\mathbf{B_1}(\mathbf{r}) \cdot \gamma \cdot \langle\downarrow|\mathbf{S}|\uparrow\rangle$ is spatially inhomogeneous, reaching its largest value close to the inductance [see Fig. 1(b)]. The spins are probed by sending microwave pulses at pulsation ω_0 through the heavily attenuated input line; the reflected pulses, together with the subsequent spin fluorescence signal, are routed via a circulator toward a SMPD based on a superconducting transmon qubit [4,20]. The sample and SMPD are cooled at 10 mK in a dilution refrigerator. The SMPD is operated cyclically, each cycle giving a click or not. Two different SMPD devices were used in this Letter, with different cycle duration and dark count rates (see Methods).

Upon application of a microwave pulse (amplitude β at the resonator input and duration Dt), the spins undergo a Rabi nutation, which leaves them in their excited state with a certain probability. Since the nutation (Rabi) frequency of

a spin is proportional to its coupling constant g_0, which is spatially inhomogeneous [see Fig. 1(b)], we are unable to apply a well-defined rotation to all spins, leading to a reduced echo contrast compared with the ideal Hahn echo sequence, as we shall see below. After the pulse, each excited spin has a certain probability to relax into its ground state by emitting a microwave photon, which may then be detected by the SMPD. We count the number of clicks recorded by the SMPD during an integration time T_{int} following the microwave pulse (or pulse sequence) and subtract the dark count background, yielding the spin signal C_{spin} (see the Supplemental Material [30] for more details). Repeating the same sequence a large number of times with repetition time T_{rep}, we obtain the probability distribution to find a number of counts $p(C_{\mathrm{spin}})$, from which we can extract the ensemble-averaged value $\langle C_{\mathrm{spin}}\rangle$ as well as the standard deviation σ. In the limit where the integration time T_{int} is long compared with the inverse spin radiative rate Γ_R^{-1} and where all spins relax radiatively, the ensemble-averaged number of counts $\langle C_{\mathrm{spin}}\rangle \approx \eta[2\langle S_Z\rangle + 1]/2$ directly yields the spin ensemble longitudinal magnetization S_Z after the pulse, $\eta = 0.1 \pm 0.01$ being the probability that an excited spin gives rise to a detected count as calibrated in separate measurements (see Methods). A more detailed analysis, quantitatively taking into account the possibility of nonradiative spin relaxation, and the spread in spin excitation probability and radiative relaxation rates due to the spatial dependence of the coupling constant g_0 throughout the sample, can be found in the Methods and is used in the simulations described below.

For spectroscopy, we measure $\langle C_{\mathrm{spin}}\rangle$ as a function of the magnetic field B_0, applied at an angle $\varphi = 30°$ with respect to the a axis in the ab plane which minimizes the erbium linewidth [31]. As shown in Fig. 1(d), a peak is observed around $B_0 = 59$ mT, corresponding to the erbium resonance. An approximately Lorentzian line shape is obtained, with FWHM 1.6 MHz, in agreement with the results obtained by ID EPR [25].

We now turn to the fluorescence detection of spin echoes. The sequence consists of one pulse of amplitude $\beta/2$ around the X axis, followed after a delay τ by a second pulse of amplitude β around the Y axis, and after another delay τ by a third pulse of amplitude $\beta/2$ around an axis making a variable angle Φ with X. In Fig. 2(a), the ensemble-averaged number of counts $\langle C_{\mathrm{spin}}\rangle$ is shown as a function of Φ. The data are well fitted by $\langle C_{\mathrm{spin}}(\Phi)\rangle = \langle C_0\rangle + \langle C_e\rangle \cos\Phi$, thus displaying the expected FD-echo coherent modulation. The FD echo amplitude is obtained by successively measuring the number of counts for $\Phi = 0$ and $\Phi = \pi$, yielding $C_e \equiv [C_{\mathrm{spin}}(0) - C_{\mathrm{spin}}(\pi)]/2$. Varying the delay $\tau + \Delta\tau$ between the second and third pulses, $\langle C_e\rangle$ shows a clear echo shape with $T_e = 6.1$ μs [see Fig. 2(b)].

Whereas the model with ideal pulses predicts a fully contrasted modulation ($\langle C_e\rangle = \langle C_0\rangle$), we observe

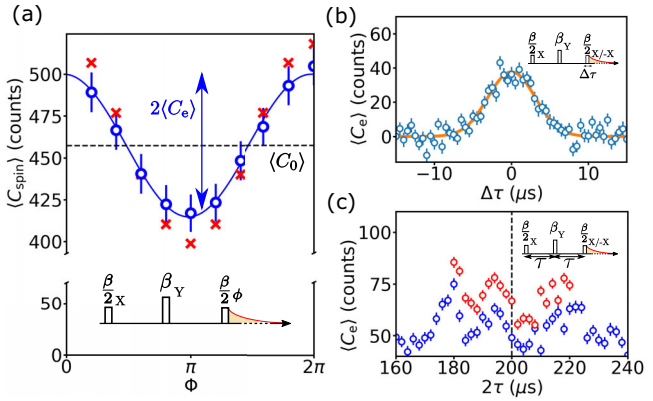

FIG. 2. Fluorescence detection of spin echo. Error bars are 1σ statistical. Data were obtained with SMPD1. Insets represent the pulse sequence used for each dataset. (a) Integrated counts with background subtracted $\langle C_{\mathrm{spin}}\rangle$ as a function of the restoring pulse phase Φ. Blue open circles (red crosses) are experimental (simulated) points, with $\tau = 100$ μs, $T_{\mathrm{rep}} = T_{\mathrm{int}} = 1.52$ s, $\beta = 10$ ns$^{-1/2}$, $\Delta t = 5$ μs, and $\eta = 0.1$. The solid line is a fit yielding $\langle C_e\rangle = 42.6$ counts (blue double arrow) and $\langle C_0\rangle = 457.3$ counts (horizontal black dashed line). (b) $\langle C_e\rangle$ (open blue dots) as a function of delay $\Delta\tau$ with $\beta = 28$ ns$^{-1/2}$, $\Delta t = 5$ μs, and $T_{\mathrm{int}} = T_{\mathrm{rep}} = 1.52$ s. The solid line is a Gaussian fit yielding $T_e = 6.1$ μs. (c) $\langle C_e\rangle$ as a function of delay 2τ showing ESEEM, with $\beta = 10$ ns$^{-1/2}$, $\Delta t = 5$ μs, and $T_{\mathrm{int}} = T_{\mathrm{rep}} = 1.52$ s. The vertical dashed line is $\tau = 100$ μs used in (a). The blue and red open circles are the results from two successive runs.

that $\langle C_e\rangle \ll \langle C_0\rangle$, which calls for an explanation. Simulations of the spin ensemble dynamics under the three-pulse sequence (see the Supplemental Material [30]), rescaled by the known efficiency η, are visible in Fig. 2(a). They show an oscillation with the same phase as the data, a slightly larger amplitude, and an offset close to the measured $\langle C_0\rangle$. This indicates that the reduced contrast is mainly due to the spread in flip (Rabi) angles among the spin ensemble, which could be mitigated in future work using rapid adiabatic pulses [32–38].

An important application of spin echoes is to probe the local environment of paramagnetic species through pulsed hyperfine spectroscopy [1]. We now show that this is possible also with FD, by measuring the modulation of the Er^{3+} echo signal caused by the proximal nuclear spin environment [21,39,40]. In Fig. 2(c), we plot $\langle C_e\rangle$ as a function of the interpulse delay τ with a 1 μs step size. We observe a reproducible modulation, likely due to the hyperfine coupling of the erbium electron spin to the proximal ^{183}W nuclear spins [41]. We note that the echo modulation also possibly explains the reduction in echo amplitude of the measurements in Fig. 2(a) with respect to the simulations (which do not take ESEEM into account), as the chosen interpulse delay $\tau = 100$ μs in Fig. 2(a) is close to an ESEEM minimum, as seen in Fig. 2(c).

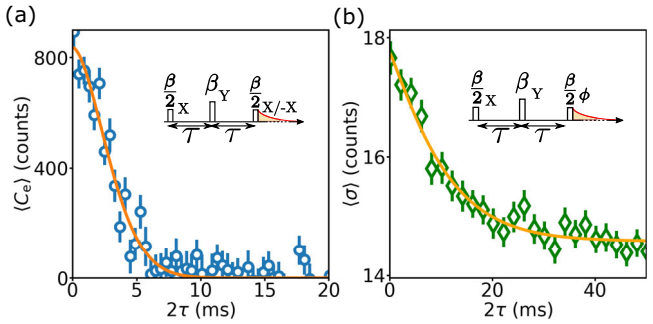

FIG. 3. Fluorescence detection of the spin coherence time. Error bars are 1σ statistical. Data were obtained with SMPD1. (a) $\langle C_e \rangle$ as a function of the echo delay 2τ (blue open circles) with $\beta = 100\ \mathrm{ns}^{-1/2}$, $\Delta t = 5\ \mu\mathrm{s}$, and $T_{\mathrm{int}} = T_{\mathrm{rep}} = 8.16$ s. The orange line is a fit yielding $T_{2,q} = 3.6$ ms and exponent $x_q = 1.7$. (b) Standard deviation $\langle \sigma \rangle$ over the phases $\Phi \in [0, \pi/2, \pi, 3\pi/2]$ as a function of the delay 2τ (green open diamonds) with $\beta = 10\ \mathrm{ns}^{-1/2}$, $\Delta t = 5\ \mu\mathrm{s}$, $T_{\mathrm{int}} = 0.55$ s, and $T_{\mathrm{rep}} = 1.52$ s. The orange line is a stretched exponential fit, yielding the coherence time $T_{2,m} = 19$ ms and exponent $x_m = 1.13$.

Using the FD echo, we can measure the Er^{3+} spin coherence time. First, we measure $\langle C_e \rangle$ as a function of the interpulse delay τ [see Fig. 3(a)]. The data are fitted by a stretched exponential decay $\langle C_e \rangle = A e^{-(2\tau/T_{2,q})^{x_q}}$, yielding a time constant $T_{2,q} = 3.6$ ms and exponent $x_q = 1.7$. This is consistent with the values measured in Ref. [25] using ID EPR in quadrature-averaged mode. It was found in Ref. [25] that this decay is due to global magnetic field noise which randomizes the echo phase from shot to shot; and from Fig. 2(a), it is clear that the echo signal in $\langle C_e \rangle$ in our three-pulse sequence is indeed sensitive to noise in the relative phase Φ. In ID EPR, the (longer) intrinsic spin coherence time $T_2 = 23$ ms was retrieved by averaging in magnitude the ID echo signal [25]. In our FD echo detection sequence, we similarly retrieve the intrinsic spin coherence time by measuring the decay of the standard deviation of the number of counts $\sigma(\tau)$ (see the Supplemental Material [30]). We thus measure the total count $C(\Phi_k, \tau)$ as a function of τ for $\Phi_k = k\pi/2$ $(k = 0, 1, 2, 3)$ and compute the standard deviation at a given τ over the four angles Φ_k.The data averaged over 950 repetitions [shown in Fig. 3(c)] are fitted with $\langle \sigma \rangle = \sqrt{A e^{-2(2\tau/T_{2,m})^{x_m}} + B}$ (see the Supplemental Material [30]) and yield the spin coherence time $T_{2,m} = 19$ ms and stretching exponent $x_m = 1.13$. The value of $T_{2,m}$ is in good agreement with the one obtained by ID echo and magnitude averaging [42,43] as well as with expectations from spectral diffusion caused by the ^{183}W nuclear spin bath dynamics [25]; the fitted stretching exponent is lower, for unknown reasons.

We finally compare the SNR of FD and ID echo. For that, the setup is modified as shown in Fig. 4(a): a nondegenerate Josephson parametric amplifier (JPA) is included in the measurement chain behind the SMPD2. This makes it possible to measure the SNR of ID two-pulse and FD restored-echo sequences in identical conditions (first-two-pulse amplitude and duration, as well as repetition time). To avoid JPA saturation, we use much lower pulse powers than in Fig. 1 measurements, leading to a larger relaxation rate $\Gamma_R \sim 10\ \mathrm{s}^{-1}$ (data not shown). The resulting echo histograms are shown in Fig. 4(b), both for ID and FD, for a total measurement time of 8.6 s, corresponding to the averaging of $N_s = 20$ consecutive sequences. Both sets of data are fitted with a Gaussian to deduce their statistics.

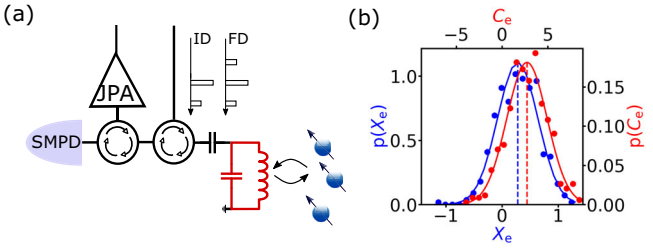

FIG. 4. SNR comparison between ID and FD detection methods. (a) Setup. A JPA is installed behind the SMPD2 for ID echo measurement. B_0 is applied with an angle $\varphi = 47°$. (b) Echo histograms detected with FD (red dots, 4000 iterations) and ID (blue dots, 9000 iterations) taken in the same conditions with $\beta \approx 2.5\ \mathrm{ns}^{-1/2}$ and $\Delta t = 4\ \mu\mathrm{s}$, and their Gaussian fits (line). The data have been averaged over 20 iterations, corresponding to a measurement time of 8.6 s. The horizontal axes for FD and ID detection are chosen such that the standard deviations have the same width, to allow for visual comparison of the distributions' mean (dashed lines).

We first note that $\langle X_e \rangle^2 = 0.08$, whereas $\langle C_e \rangle = 2.7$, confirming that a larger number of photons can indeed be obtained with FD than with ID echo. The standard deviation of the ID echo is found to be $\delta X_e = 0.39$. This is close to, although larger than, the value $1/\sqrt{2N_s} = 0.16$ expected from the sole contribution of vacuum fluctuations and added noise from the quantum-limited amplifier, likely due to contributions from other amplifiers in the detection chain, as well as a possible overestimation of the echo photon number conversion factor (see the Supplemental Material [30]). The standard deviation of the FD echo $\delta C_e = 2.2$ counts is, on the other hand, dominated by the dark count contribution. Despite that, the measured FD echo signal-to-noise ratio $\langle C_e \rangle / \delta C_e = 1.25 \pm 0.10$ is larger than the ID echo $\langle X_e \rangle / \delta X_e = 0.73 \pm 0.09$. Using the simulation to evaluate the number of spins excited during the echo sequence, we get a spin detection sensitivity of $7.5 \times 10^2\ \mathrm{spin}/\sqrt{\mathrm{Hz}}$ with FD and $1.2 \times 10^3\ \mathrm{spin}/\sqrt{\mathrm{Hz}}$ with ID. This confirms the interest of fluorescence detection when applied to echo detection, even with the present generation of SMPD devices. Future SMPDs with lower dark count rates would yield further enhancements; for instance, SMPD1 in the same operating conditions would

double the signal-to-noise ratio, given its 4 times lower dark count rate [4]. Note that this quantitative comparison was not measured with SMPD1 due to the absence of a parametric amplifier in the spin detection chain.

The detection of spin echoes using fluorescence detection completes the proof-of-principle results in Ref. [4] and establishes FD EPR as an operational alternative to ID EPR. To reach its full potential, FD EPR requires spins in the Purcell regime, implying that they should be located within the picoliter resonator mode volume. Therefore, FD EPR may prove useful for samples with small volumes, such as two-dimensional materials. Finally, with larger radiative rate and lower dark count SMPD devices, FD EPR has the potential to reach single-spin sensitivity in the near future [44].

We acknowledge technical support from P. Sénat, P.-F. Orfila, and S. Delprat, and are grateful for fruitful discussions within the Quantronics group. We acknowledge IARPA and Lincoln Labs for providing a JTWPA used in the measurements. We acknowledge support from the Agence Nationale de la Recherche (ANR) through projects MIRESPIN (ANR-19-CE47-0011), DARKWADOR (ANR-19-CE47-0004), MARS (ANR-20-CE92-0041), and through the Chaire Industrielle NASNIQ (ANR-17-CHIN-0001) cofunded by Atos, and from the Région Ile-De-France through the DIM SIRTEQ (project REIMIC). This project has received funding from the European Union's Horizon 2020 research and innovation program under Marie Sklodowska-Curie Grant Agreement No. 792727 (SMERC). S. B. thanks the support of the CNRS research infrastructure INFRANALYTICS (FR 2054).

*patrice.bertet@cea.fr
†emmanuel.flurin@cea.fr

[1] A. Schweiger and G. Jeschke, *Principles of Pulse Electron Paramagnetic Resonance* (Oxford University Press, New York, 2001).
[2] E. L. Hahn, Spin echoes, Phys. Rev. **80**, 580 (1950).
[3] A. Bienfait, J. J. Pla, Y. Kubo, M. Stern, X. Zhou, C. C. Lo, C. D. Weis, T. Schenkel, M. L. W. Thewalt, D. Vion, D. Esteve, B. Julsgaard, K. Moelmer, J. J. L. Morton, and P. Bertet, Reaching the quantum limit of sensitivity in electron spin resonance, Nat. Nanotechnol. **11**, 253 (2016).
[4] E. Albertinale, L. Balembois, E. Billaud, V. Ranjan, D. Flanigan, T. Schenkel, D. Estève, D. Vion, P. Bertet, and E. Flurin, Detecting spins by their fluorescence with a microwave photon counter, Nature (London) **600**, 434 (2021).
[5] J. Wrachtrup, C. Von Borczyskowski, J. Bernard, M. Orritt, and R. Brown, Optical detection of magnetic resonance in a single molecule, Nature (London) **363**, 244 (1993).
[6] J. J. Pla, K. Y. Tan, J. P. Dehollain, W. H. Lim, J. J. L. Morton, D. N. Jamieson, A. S. Dzurak, and A. Morello, A single-atom electron spin qubit in silicon, Nature (London) **489**, 541 (2012).
[7] D. Rugar, R. Budakian, H. Mamin, and B. Chui, Single spin detection by magnetic resonance force microscopy, Nature (London) **430**, 329 (2004).
[8] M. Grinolds, M. Warner, K. De Greve, Y. Dovzhenko, L. Thiel, R. Walsworth, S. Hong, P. Maletinsky, and A. Yacoby, Subnanometre resolution in three-dimensional magnetic resonance imaging of individual dark spins, Nat. Nanotechnol. **9**, 279 (2014).
[9] R. Narkowicz, D. Suter, and I. Niemeyer, Scaling of sensitivity and efficiency in planar microresonators for electron spin resonance, Rev. Sci. Instrum. **79**, 084702 (2008).
[10] L. Shtirberg, Y. Twig, E. Dikarov, R. Halevy, M. Levit, and A. Blank, High-sensitivity Q-band electron spin resonance imaging system with submicron resolution, Rev. Sci. Instrum. **82**, 043708 (2011).
[11] H. Malissa, D. I. Schuster, A. M. Tyryshkin, A. A. Houck, and S. A. Lyon, Superconducting coplanar waveguide resonators for low temperature pulsed electron spin resonance spectroscopy, Rev. Sci. Instrum. **84**, 025116 (2013).
[12] A. J. Sigillito, H. Malissa, A. M. Tyryshkin, H. Riemann, N. V. Abrosimov, P. Becker, H.-J. Pohl, M. L. W. Thewalt, K. M. Itoh, J. J. L. Morton, A. A. Houck, D. I. Schuster, and S. A. Lyon, Fast, low-power manipulation of spin ensembles in superconducting microresonators, Appl. Phys. Lett. **104**, 222407 (2014).
[13] Y. Artzi, Y. Twig, and A. Blank, Induction-detection electron spin resonance with spin sensitivity of a few tens of spins, Appl. Phys. Lett. **106**, 084104 (2015).
[14] A. Bienfait, J. Pla, Y. Kubo, X. Zhou, M. Stern, C.-C. Lo, C. Weis, T. Schenkel, D. Vion, D. Esteve, J. Morton, and P. Bertet, Controlling spin relaxation with a cavity, Nature (London) **531**, 74 (2016).
[15] C. Eichler, A. J. Sigillito, S. A. Lyon, and J. R. Petta, Electron Spin Resonance at the Level of 10^4 Spins Using Low Impedance Superconducting Resonators, Phys. Rev. Lett. **118**, 037701 (2017).
[16] S. Probst, A. Bienfait, P. Campagne-Ibarcq, J. J. Pla, B. Albanese, J. F. D. S. Barbosa, T. Schenkel, D. Vion, D. Esteve, K. Moelmer, J. J. L. Morton, R. Heeres, and P. Bertet, Inductive-detection electron-spin resonance spectroscopy with 65 spins/$\mathrm{Hz}^{(1/2)}$ sensitivity, Appl. Phys. Lett. **111**, 202604 (2017).
[17] V. Ranjan, S. Probst, B. Albanese, T. Schenkel, D. Vion, D. Esteve, J. J. L. Morton, and P. Bertet, Electron spin resonance spectroscopy with femtoliter detection volume, Appl. Phys. Lett. **116**, 184002 (2020).
[18] W. G. Breiland, C. B. Harris, and A. Pines, Optically Detected Electron Spin Echoes and Free Precession in Molecular Excited States, Phys. Rev. Lett. **30**, 158 (1973).
[19] E. v. Oort, N. B. Manson, and M. Glasbeek, Optically detected spin coherence of the diamond N-V centre in its triplet ground state, J. Phys. C **21**, 4385 (1988).
[20] R. Lescanne, S. Deléglise, E. Albertinale, U. Réglade, T. Capelle, E. Ivanov, T. Jacqmin, Z. Leghtas, and E. Flurin, Irreversible Qubit-Photon Coupling for the Detection of Itinerant Microwave Photons, Phys. Rev. X **10**, 021038 (2020).
[21] W. B. Mims, K. Nassau, and J. D. McGee, Spectral diffusion in electron resonance lines, Phys. Rev. **123**, 2059 (1961).

[22] A. Antipin, A. Katyshev, I. Kurkin, and L. Shekun, Paramagnetic resonance and spin-lattice relaxation of Er3+ and Tb3+ ions in CaWO4 crystal lattice, Sov. Phys. Solid State **10**, 468 (1968).
[23] B. G. Enrique, Optical spectrum and magnetic properties of Er3+ in CaWO4, J. Chem. Phys. **55**, 2538 (1971).
[24] S. Bertaina, S. Gambarelli, A. Tkachuk, I. N. Kurkin, B. Malkin, A. Stepanov, and B. Barbara, Rare-earth solid-state qubits, Nat. Nanotechnol. **2**, 39 (2007).
[25] M. Le Dantec, M. Rančić, S. Lin, E. Billaud, V. Ranjan, D. Flanigan, S. Bertaina, T. Chanelière, P. Goldner, A. Erb, R. B. Liu, D. Estève, D. Vion, E. Flurin, and P. Bertet, Twenty-three-millisecond electron spin coherence of erbium ions in a natural-abundance crystal, Sci. Adv. **7**, eabj9786 (2021).
[26] P.-Y. Li, C. Liu, Z.-Q. Zhou, X. Liu, T. Tu, T.-S. Yang, Z.-F. Li, Y. Ma, J. Hu, P.-J. Liang, X. Li, J.-Y. Huang, T.-X. Zhu, C.-F. Li, and G.-C. Guo, Hyperfine Structure and Coherent Dynamics of Rare-Earth Spins Explored with Electron-Nuclear Double Resonance at Subkelvin Temperatures, Phys. Rev. Appl. **13**, 024080 (2020).
[27] M. Rančić, M. Le Dantec, S. Lin, S. Bertaina, T. Chanelière, D. Serrano, P. Goldner, R. B. Liu, E. Flurin, D. Estève, D. Vion, and P. Bertet, Electron-spin spectral diffusion in an erbium doped crystal at Millikelvin temperatures, Phys. Rev. B **106**, 144412 (2022).
[28] J. Alexander, G. Dold, O. W. Kennedy, M. Šimėnas, J. O'Sullivan, C. W. Zollitsch, S. Welinski, A. Ferrier, E. Lafitte-Houssat, T. Lindström, P. Goldner, and J. J. L. Morton, Coherent spin dynamics of rare-earth doped crystals in the high-cooperativity regime, Phys. Rev. B **106**, 245416 (2022).
[29] A. Erb and J.-C. Lanfranchi, Growth of high-purity scintillating CaWO4 single crystals for the low-temperature direct dark matter search experiments CRESST-II and EURECA, Cryst. Eng. Commun. **15**, 2301 (2013).
[30] See Supplemental Material at http://link.aps.org/supplemental/10.1103/PhysRevLett.131.100804 for more details on the data acquisition, and on the measurement of the coherence time through the time-dependence of the fluorescence signal standard deviation.
[31] W. B. Mims and R. Gillen, Broadening of paramagnetic-resonance lines by internal electric fields, Phys. Rev. **148**, 438 (1966).
[32] A. Doll and G. Jeschke, Wideband frequency-swept excitation in pulsed EPR spectroscopy, J. Magn. Reson. **280**, 46 (2017).
[33] A. Doll, S. Pribitzer, R. Tschaggelar, and G. Jeschke, Adiabatic and fast passage ultra-wideband inversion in pulsed EPR, J. Magn. Reson. **230**, 27 (2013).
[34] P. E. Spindler, P. Schöps, W. Kallies, S. J. Glaser, and T. F. Prisner, Perspectives of shaped pulses for EPR spectroscopy, J. Magn. Reson. **280**, 30 (2017), Special Issue on Methodological advances in EPR spectroscopy and imaging.
[35] J. O'Sullivan, O. W. Kennedy, K. Debnath, J. Alexander, C. W. Zollitsch, M. Šimėnas, A. Hashim, C. N. Thomas, S. Withington, I. Siddiqi, K. Mølmer, and J. J. L. Morton, Random-Access Quantum Memory Using Chirped Pulse Phase Encoding, Phys. Rev. X **12**, 041014 (2022).
[36] S. Mieth, D. Schraft, T. Halfmann, and L. P. Yatsenko, Rephasing of optically driven atomic coherences by rapid adiabatic passage in $Pr3+:Y2SiO5$, Phys. Rev. A **86**, 063404 (2012).
[37] M. F. Pascual-Winter, R. C. Tongning, R. Lauro, A. Louchet-Chauvet, T. Chanelière, and J.-L. Le Gouët, Adiabatic passage with spin locking in Tm3 + YAG, Phys. Rev. B **86**, 064301 (2012).
[38] D. Schraft, T. Halfmann, G. T. Genov, and N. V. Vitanov, Experimental demonstration of composite adiabatic passage, Phys. Rev. A **88**, 063406 (2013).
[39] W. B. Mims, Envelope modulation in spin-echo experiments, Phys. Rev. B **5**, 2409 (1972).
[40] W. B. Mims, J. L. Davis, and J. Peisach, The exchange of hydrogen ions and of water molecules near the active site of cytochrome c, J. Magn. Reson. (1969) **86**, 273 (1990).
[41] S. Probst, G. Zhang, M. Rančić, V. Ranjan, M. Le Dantec, Z. Zhang, B. Albanese, A. Doll, R. B. Liu, J. Morton, T. Chanelière, P. Goldner, D. Vion, D. Esteve, and P. Bertet, Hyperfine spectroscopy in a quantum-limited spectrometer, Magn. Reson. **1**, 315 (2020).
[42] A. M. Tyryshkin, S. A. Lyon, A. V. Astashkin, and A. M. Raitsimring, Electron spin relaxation times of phosphorus donors in silicon, Phys. Rev. B **68**, 193207 (2003).
[43] A. M. Tyryshkin, S. Tojo, J. J. L. Morton, H. Riemann, N. V. Abrosimov, P. Becker, H.-J. Pohl, T. Schenkel, M. L. W. Thewalt, K. M. Itoh, and S. A. Lyon, Electron spin coherence exceeding seconds in high-purity silicon, Nat. Mater. **11**, 143 (2012).
[44] Z. Wang, L. Balembois, M. Rančić, E. Billaud, M. L. Dantec, A. Ferrier, P. Goldner, S. Bertaina, T. Chanelière, D. Estève, D. Vion, P. Bertet, and E. Flurin, Single electron-spin-resonance detection by microwave photon counting, Nature **619**, 276 (2023).